Fisheries Research 228 (2020) 105568

Contents lists available at ScienceDirect

Fisheries Research

journal homepage: www.elsevier.com/locate/fishres

Remote sizing of fish-like targets using broadband acoustics

Rokas Kubilius*, Gavin J. Macaulay, Egil Ona

Institute of Marine Research, P.O. Box 1870 Nordnes, NO-5817 Bergen, Norway

ARTICLE INFO

Handled by: George A. Rose

Keywords:
Acoustic
Broadband
Echosounder
Fish
Size

ABSTRACT

Broadband echosounder systems provide very high range resolution that could resolve different parts of fish and hence provide estimates of fish size. The potential for, and accuracy of, direct acoustic sizing of fish was tested on fish-like targets of known dimensions and orientations. Prolate spheroids, 91–477 mm long, with and without an air-filled inclusion (simulating a fish swim-bladder), made from polyvinyl-alcohol-cryogel, were suspended in an acoustic beam and rotated while the backscattered signal was recorded. The echoes from linear frequency modulated pulses of 45 – 90 and 160 – 260 kHz with a fast and a slow amplitude modulation were pulse-compressed to provide data with a range resolution of 6.6 mm at its highest. Echoes from the target boundaries were manually identified, tracked and used to directly estimate the thickness and length of the targets. An accuracy of ± 11 – 17 mm was achieved for targets longer than about 200 mm and thicker than about 20 mm when using the 160 – 260 kHz pulse. The length of the air-filled inclusion could also be estimated for the larger targets. Echoes from the slow amplitude modulation were easier to interpret than the fast amplitude modulation despite the lower range resolution, due to the lower pulse compression temporal sidelobes. The results show that remote acoustic sizing of fish is feasible and of sufficient accuracy for practical use.

1. Introduction

Oceanic pelagic trawling and purse seine fishing accounts for about 20 % and 30 % respectively of the global landings of pelagic fishes (Watson et al., 2006). Echosounders and omni-directional sonars are the main tool to find fish in those fisheries. In purse seining, for example, omni-directional sonar is the primary tool to locate fish schools of interest. However, seining is unselective after the school is surrounded by the seine, with respect to species, fish size and quality (e.g. fat content). The release of unwanted catch is a common practice in purse seining and can cause very high mortality in the released fish (e.g., Huse and Vold, 2010; Tenningen et al., 2012). In a similar manner, pre-catch knowledge of fish size is important during pelagic trawling operations as undersized and/or low-quality fish can lead to financially unsustainable operations. Obtaining organism size estimates without biological sampling is also of interest for autonomous platforms such as surface and underwater drones. There are few effective methods to conveniently obtain this size and quality information, apart from acoustic techniques, which have a sufficiently large operating range. Optical instruments are a potential sizing tool, but due to their limited operating range require deployment from a vessel with the additional complexities that this entails, and we focus here on the development of acoustic techniques.

Fish sizing with active acoustics is mostly limited to the use of average target strength to fish length relationships established from, and applied to, large numbers of fish echoes. The stochastic nature of target strength means that a few echoes from an individual fish cannot reliably be used to size that fish from a target strength to fish length relationship (Simmonds and MacLennan, 2005). Narrowband acoustic pulses (defined here as having a bandwidth that is less than about 10 % of the nominal frequency) have a range resolution that is proportional to half the pulse duration (defined as the separation distance between two targets that allows both to be resolved as separate). For example, a 1 ms pulse has a range resolution of about 0.75 m (at a sound speed of 1500 m s^{-1}), which is too large to resolve the parts of many commercially fished species, such as Atlantic herring or mackerel. Shorter pulse durations, such as 64 µs (range resolution of about 48 mm) could resolve parts of large fish, but at commonly used frequencies (18 – 200 kHz) the echo suffers from poor a signal-to-noise ratio and hence has a limited useful range. Considerably higher range resolutions can be obtained with the shorter pulses that are feasible in higher frequency systems (e.g., more than about 600 kHz) (Belcher et al., 2001; Söhnlein et al., 2011; Briseño-Avena et al., 2015; Chu et al., 2015), but the effective range is several meters at most and of little use for oceanic applications on mobile fish, unless they are used on drones, probes or alike.

* Corresponding author.
E-mail address: rokas@hi.no (R. Kubilius).

https://doi.org/10.1016/j.fishres.2020.105568
Received 23 October 2019; Received in revised form 16 March 2020; Accepted 22 March 2020
Available online 27 April 2020

Broadband signals have an advantage over narrow-band signals in that the use of frequency modulated signals and associated pulse compression (most commonly matched filtering) gives a range resolution that is inversely proportional to twice the bandwidth of the signal (Ehrenberg and Torkelson, 2000; Stanton et al., 2003). This can give a range resolution that can resolve the echoes from different parts of a fish yet retain a useful working range. A disadvantage of pulse compression is the presence of temporal sidelobes in the pulse compressed signal – these can obscure echoes from adjacent objects, however, the broadband pulse shape can be weighted to adjust the level of these sidelobes (Cook and Bernfeld, 1967). Multi-view acoustic systems have shown promise for sizing organisms (Jaffe, 2006) and inferring orientation (Jaffe and Roberts, 2011) but the requirement to receive the backscatter at multiple angles is problematic for practical oceanic use.

Broadband acoustic pulses with high spatial resolution are commonly used for medical ultrasound imaging (Chan and Perlas, 2011) and can resolve detailed anatomical structures of fish (Chu et al., 2015) and hence provide size estimates. However, the very high operating frequencies of these systems (several MHz) results in short operating ranges (less than a few meters).

Broadband scattering from an individual fish is complex (see e.g., Macaulay, 2002; Au and Benoit-Bird, 2003; Imaizumi et al., 2008; Forland et al., 2014). The multitude of impedance contrasts between body parts such as the bones, flesh, liver, and swim-bladder result in a dynamic acoustic scattering environment. An added complexity is the constructive and destructive interference of echoes across the pulse bandwidth and as the fish moves. The increased range resolution available from pulse compressed broadband signals could be used to characterise the target beyond the echo amplitude and coarse frequency response that are commonly used for echo classification purposes. The potential exists to more precisely identify fish species, estimate body fat content, determine maturity state or to directly measure fish body size, as suggested by Jaffe and Roberts (2011). The complexity of the scattering from fish, however, also makes it difficult to take the first step to understand the feasibility and accuracy of the direct acoustic sizing of individual fish. This can be addressed via modelling (e.g., Stanton et al., 2018) or experimental approaches. Here an experimental approach is taken, and to further simply the problem, we use artificial targets of known shapes and sizes with similar backscattering properties as fish flesh.

In this paper we demonstrate that, i) pulse-compressed broadband signals can provide a spatial range resolution that is high enough to resolve the dimensions of medium-sized fishes, ii) the boundaries of fish-flesh-like objects can be separated and identified within the total scattering from the target, and iii) the length and thickness of a fish-flesh-like target can be inferred and measured remotely and directly. We also provide estimates of the accuracy and applicability of direct acoustic fish sizing.

2. Material and methods

Artificial fish-flesh-like objects (henceforth called targets) with and without an air-filled cavity were ensonified with broadband acoustic pulses in seawater (Fig. 1). The methods and apparatus used to do this are described below.

2.1. Targets

Eighteen prolate spheroids with an aspect ratio of approximately 4:1 were cast from polyvinyl alcohol cryogel (PVA-C). The length varied between 91 and 477 mm (Table 1). Nine of the targets were internally homogenous and simulated fish flesh (referred to as 'plain' or 'PL' targets). The other nine targets contained a cavity (also prolate spheroid in shape) that simulated the gas-filled swim-bladders found in some species of fish (referred to as 'SB' targets).

Two-sided mould negatives were made from silicone rubber (Fig. 2) poured around hard plastic prolate spheroids machined to an accuracy ±0.5 mm. The cured silicone had a Shore A hardness of 24, which was hard enough to keep its' shape, but soft enough to form a seal that prevented PVA gel leakage during casting. The two mould negatives were gently held together with wood plates and clamps.

PVA powder (hydrolyzation 99 %) was dissolved in a 1:9 ratio by weight with ~90 °C temperature water and then cooled to room temperature. To ensure a 10 % by weight gel was produced, the weight of the cooled gel was measured and any loss due to evaporation remedied by adding more water. The gel was stored in air-tight containers for up to three days before being gently poured into moulds and left to rest for 10 − 12 h to allow any air bubbles to rise. The gel was then solidified using four freeze-thaw cycles (Surry et al., 2004). For targets of 91 − 280 mm length each cycle was 12 h at -20 °C followed by 12 h at room temperature (approximately 20 °C). Targets longer than 280 mm used a 36/36 h cycle to allow for complete freezing and thawing. The transverse cross-section of casts longer than 250 mm became slightly oval due to the way the moulds were oriented during freezing/thawing. Targets with a cavity were produced by suspending a solid plastic prolate spheroid in the PVA gel for the first two freeze-thaw cycles (Fig. 2, right panel), then removing it via an incision which was sealed by applying additional PVA gel to the incision prior to the remaining freeze-thaw cycles. Completed targets were stored in freshwater until use (Surry et al., 2004). Target length, maximum width and height of the targets were measured just before or after acoustic measurements.

Density and sound speed in selected targets were measured. The volume of PL-2, 3 and 4 (Table 1) was measured by the water displacement method in a vertical tube to an estimated accuracy of ±1 mL. A small amount of liquid soap was added to the water to reduce the surface tension effect and the occurrence of bubbles on the target. Dry weight of the targets was measured to ±1 g and the resulting density accuracy was estimated to be ±2 kg m^{-3}. Sound speed was measured using the time-of-travel method (see e.g., Chu et al., 2000). The average time for a 500 kHz sound pulse to travel 180 mm was measured through both water and water with a target sample (from PL-1, 2, and 3; 12 − 13 mm thick slice, ±0.1 mm) sized to fully cover the acoustic beam and most of the chamber cross-section. The sound speed in the target material was estimated from the sound speed difference between water and water with the target sample of known thickness.

2.2. Site

The acoustic measurements were carried out from a floating, moored platform normally used to suspend fish net pens at the Austevoll Aquaculture Research Station, Norway, in June 2017 (Fig. 1). This provided an environment where the targets could be suspended and measured without confounding echoes from other underwater structures. The water depth below the facility was about 40 m. The equipment was installed inside of an empty net pen (12 × 12 × 12 m) that excluded unduly curious wild fish.

2.3. Target rotation

The acoustic incidence angle upon the targets was varied by rotating the target about the minor axis. To achieve this, targets were held by two loops formed as part of a horizontally stretched monofilament nylon line (diameter varied with target size from 0.10 to 0.16 mm; Figs. 1 and 2). The horizontal nylon line was connected to two vertical nylon lines (Ø0.8 mm) that ran between two horizontal steel bars (2 m, Ø30 mm, Fig. 1), the upper of which was 50 mm above the water surface and the lower 6 m below the upper. Eye bolts were installed at both ends of the upper horizontal bar, through which the vertical suspension lines passed (and were attached to small rings that prevented the vertical lines from exiting the eye bolts). This enabled us to manually lift the suspended target to the water surface, install the next target and redeploy to the same location within the acoustic beam. A vertical metal

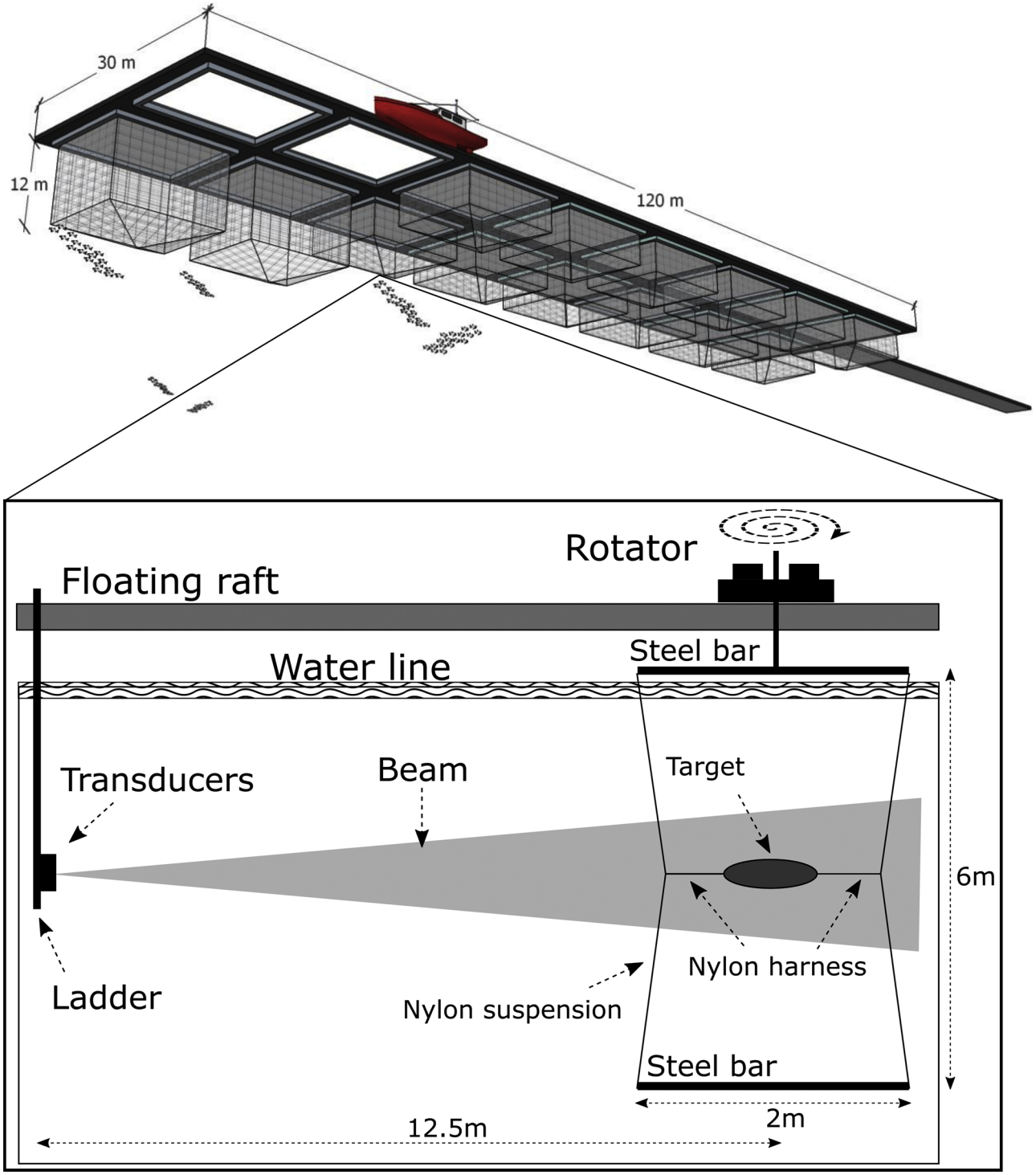

Fig. 1. Apparatus and net-pen configuration for the experiments. The rotator, target suspension setup, and echosounders (all lower) were attached to a floating net-pen platform (upper).

rod connected the centre of the upper horizontal steel bar to a rotation motor (Fig. 1).

The rotation speed and direction of the apparatus was typically set to 2.1° s^{-1} for the measurements. The motor rotation angle (and hence the suspended target), to 0.1° precision, was sent to the echosounder software at 10 Hz and incorporated into echosounder data files. Rotation angles of 0° and 180° corresponded to broadside ensonification and 90° and 270° to end-on ensonification of the targets.

2.4. Echosounder and acoustic measurements

Two broadband echosounders (Simrad EK80 transceivers and two transducers) were used to measure backscatter with simultaneous 45 − 90 and 160 − 260 kHz frequency-modulated pulses repeating at 3 Hz (Table 2). For each pulse, the echosounder offered two different tapers on the transmit pulse amplitude: 'slow' and 'fast', indicating the proportion of the pulse duration over which the transmit amplitude went from zero to maximum and maximum to zero at the end of the upsweep pulse. The slow pulse took half the pulse duration to reach

Table 1
Sizes of the PVA-C targets; length (L), maximum height (H) and width (W) and cavity length (SBL). "PL" indicates plain targets, and "SB" targets with a cavity. SBL was estimated from the proportional shrinkage of L from mould length to actual cast length.

ID	L [mm]	H [mm]	W [mm]	SBL [mm]
PL-1	465	131	119	–
PL-2	423	118	104	–
PL-3	351	101	88	–
PL-4	327	92	80	–
PL-5	280	75	68	–
PL-6	230	61	59	–
PL-7	182	46	44	–
PL-8	140	36	35	–
PL-9	91	22	23	–
SB-1	477	132	115	146
SB-2	395	110	95	132
SB-3	368	101	89	93
SB-4	312	84	75	86
SB-5	261	70	64	82
SB-6	233	61	58	94
SB-7	184	46	44	46
SB-8	135	34	33	45
SB-9	92	23	23	46

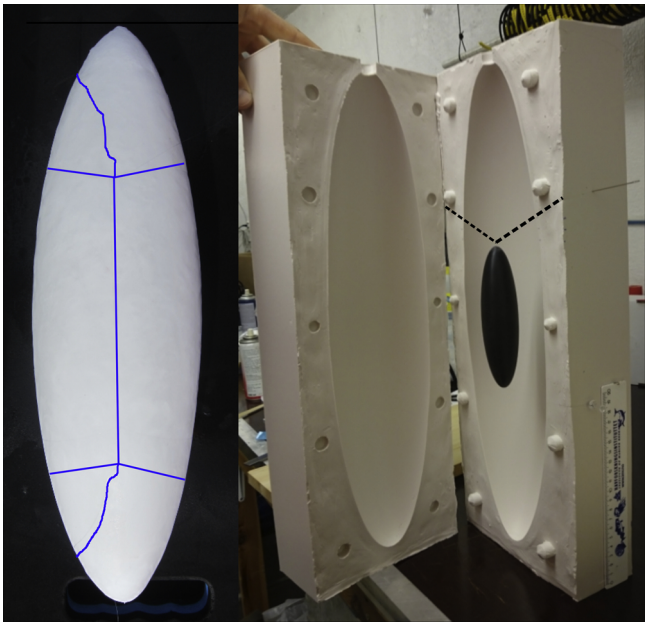

Fig. 2. PVA-C target of length 477 mm with nylon harness highlighted in blue (left) and silicone mould (right) used to produce a cavity-bearing target showing prolate spheroid (black object) suspended by nylon monofilament (highlighted by dashed line) that formed the cavity (and was removed half-way through the production process).

maximum transmit amplitude and the remaining half to reduce to zero (taper of 0.5 or 50 %). The fast pulse took 4 % of the pulse duration to reach maximum for the 45 – 90 kHz pulse and 1 % for 160 – 260 kHz (taper of 0.04 and 0.01 respectively). Data were collected with both slow and fast tapers. The echosounders were calibrated using standard methods (Demer et al., 2015) and targets (38.1 and 21 mm diameter tungsten carbide spheres with 6 % cobalt binder). The two transducers were mounted at a depth of 3 m and with approximately 230 mm horizontal centre-to-centre separation, oriented to project horizontally towards the targets. The range from the transducers to the target was about 12.8 m, well outside the echosounder nearfield and far enough for targets to be fully ensonified by the acoustic beam. The centres of the two acoustic beams were found with the use of a calibration sphere

Table 2
Echosounder and acoustic configurations. f_0 is the nominal frequency for the bandwidth (70 and 200 kHz). Sound speed estimate (at 3 m depth) was obtained daily.

Parameter		
Transducer type	ES70 – 7CD	ES200 – 7CD
Bandwidth [kHz]	45 – 90	160 – 260
Transmit power [W]	150	60
Fast power taper [%]	4	1
Slow power taper [%]	50	50
Gain at f_0 [dB]	26.8	25.0
Equivalent beam angle at f_0 [dB]	– 20.7	– 20.7
Absorption coefficient at f_0 [dB km^{-1}]	18.86	52.45
Half-power beam widths (alongship/athwartship) at f_0 [°]	6.7/6.6	6.8/6.7
Pulse duration [ms]	1.024	
Ping rate [s^{-1}]	0.33	
Sound speed [m s^{-1}]	1492.5 – 1495.2	

and the split-aperture functionality of the echosounder. The rotator and target suspension lines were then adjusted so that the targets were at the mid-point between the two beam centres. Acoustic data were stored into computer files from a minimum of four complete rotations of the target with fast and slow tapers (Table 2) – all other settings were unchanged, producing four datasets for each measured target. Conductivity and temperature profiles were taken daily to 12 m depth. Temperature and salinity at 3 m were entered into the echosounder software which then calculated sound speed (Fofonoff and Millard, 1983) and acoustic absorption (Francois and Garrison, 1982) estimates and applied these to the recorded data.

2.5. Data processing

The pulse compressed broadband acoustic data were scrutinised using the fish tracking module (based on Handegard et al., 2005; Handegard, 2007) as implemented in the LSSS software, ver. 2.6.0 (Korneliussen et al., 2016). Semi-manual fish tracking was used to create tracks that followed the two target boundary echoes and two cavity boundary echoes while the target was rotated (Fig. 3). Adjustments to the tracking algorithm were sometimes needed to maintain successful tracking in response to changes in the acoustic signal-to-noise ratio, target size, and presence of the target cavity. The base tracker settings (detailed descriptions in Handegard, 2007) were: threshold of –90 dB, maximum one-way gain compensation of –3 dB, track association settings of $\alpha_G = 2.8°$, $\beta_G = 2.8°$, $r_G = 0.01$ m, $I_G = 10$ dB, and track initiation gate of $\alpha_0 = 2.8°$, $\beta_0 = 2.8°$, $r_0 = 0.01$ m, $I_0 = 20$ dB. Here α and β are maximum accepted values for 'alongship' and 'athwartship' angles within the acoustic beam for each subsequent target detection within a track (α_G, β_G) or for initiation of a new track close to the end of a previously terminated track (α_0, β_0). r_G is a maximum shift in range from the transducer between subsequent detections within the track. r_0 is the maximum distance in range from the transducer between the last detection of a terminated track to the first detection of a new candidate track. I_G is the maximum difference in echo intensity between the subsequent detections within the track. Similarly, I_0 is maximum accepted echo intensity difference between the last detection of a terminated track and the first detection of a new candidate track. New tracks were also initiated at any point in space if several subsequent detections pass the target detection and track association settings. The maximum number of subsequent missing samples in one ping of a track was set to zero, the maximum number of subsequent missing pings in a track to two, maximum acceptable ratio of missing pings to number of pings in a track to 0.3 and the minimum acceptable total number of pings in a track to 10. The individual tracks were subsequently manually interpreted and edited to fix obvious mistakes by the tracking algorithm and joined where appropriate to

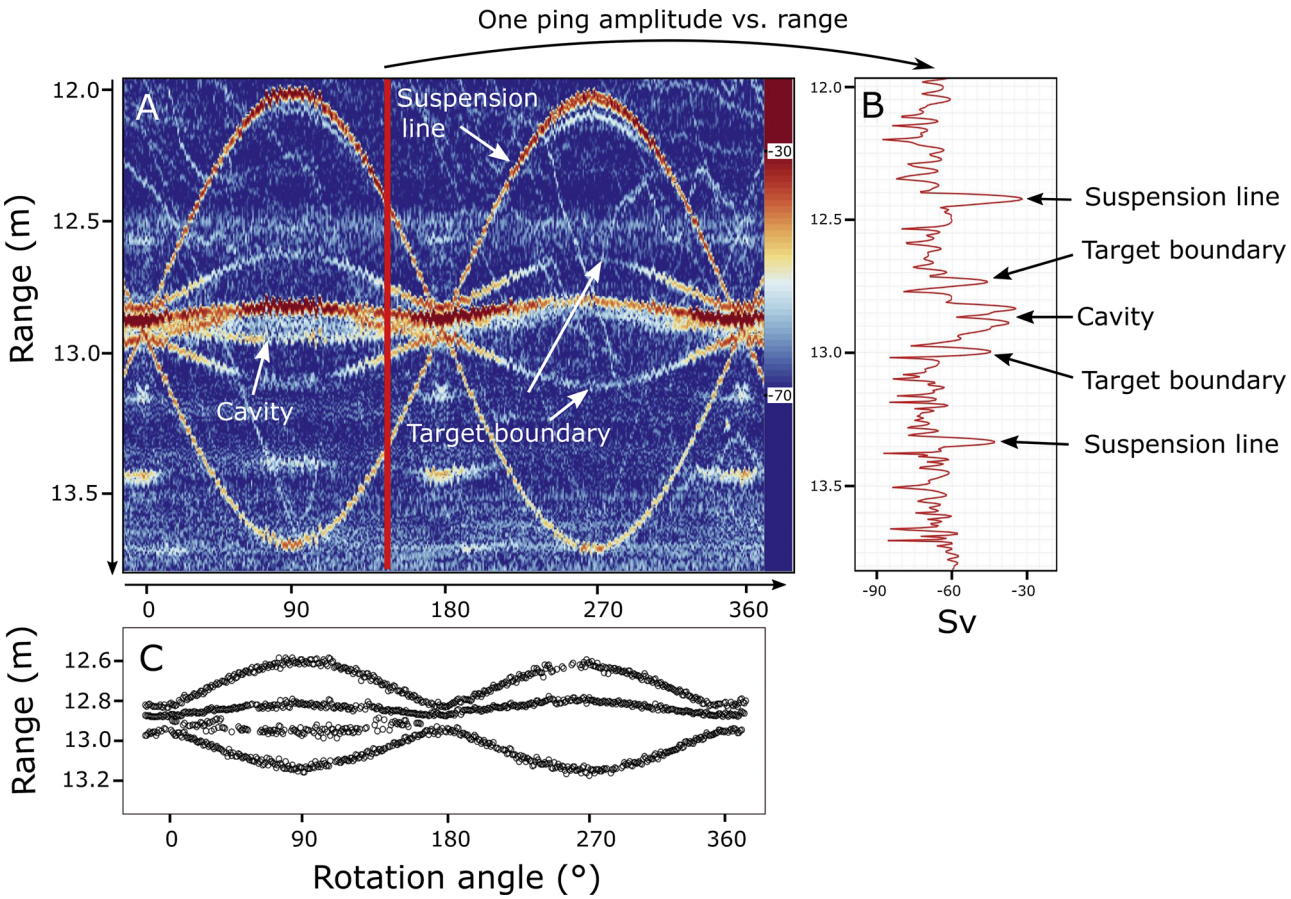

Fig. 3. An example of the echogram (A) resulting from a 360° rotation of a target (SB-1) when mounted in the rotator apparatus (using a 160-260 kHz pulse with slow taper) – the echoes generated by the target boundaries, cavity, and suspension apparatus are indicated. Detection of the echoes from the target uses the per-ping volume backscattering data (B) and results in range to target values for each ping/rotation angle (C). Rotation angles of 90° and 270° occur when the target is at the end-on to the acoustic beam. Echogram colour scale and line plot show volume backscatter strength (S_v, dB re 1 m^{-1}).

create continuous tracks for the target boundaries. Manual tracks were generated in some cases where automatic tracking algorithm returned poor results. Redundant tracks, such as those originating from drifting particles, were deleted. Note that these detected and tracked boundary echoes are a result of pulse compression of the echo returns and are representative of the target strength (TS) over the entire bandwidth of the pulse (45 – 90 or 160 – 260 kHz). The target boundary and cavity boundary echoes were considered for tracking when the TS peak had a prominence of 8 dB or more (that is, our minimum workable signal-to-noise ratio, SNR, was 8 dB).

The range to the tracks from three rotations for each target and pulse type were exported from LSSS, along with the rotation angle of the target. Estimates of apparent target size were then obtained from the difference in range between the target boundary tracks for each ping (and hence angle). The cavity size was estimated in the same manner. Estimates of actual target length and width were calculated from averages of the apparent size within 5° of the end-on and broadside angles (peaks and crests visible in Fig. 4).

2.6. Range resolution

The range resolution of a pulse compressed tapered broadband signal is inversely proportional to the bandwidth thus (Hawkins, 1996):

$$\delta x_{3dB} = \alpha_w \frac{c}{2B_C} \quad (1)$$

where δx_{3dB} is the width of the pulse compressed signal 3 dB down from the peak, c is sound speed in water, and B_C the nominal signal bandwidth. The α_w term accounts for any weighting of the broadband signal (e.g., a taper to reduce temporal sidelobes in the pulse compressed signal and to limit transient responses in the echosounder transmitter and transducer). The Simrad EK80 applies a Tukey window to transmit pulses, where the degree of tapering at the start and end of the pulse is set by a value between 0 and 0.5 (0 results in no tapering and 0.5 is equivalent to a Hann window). Values of α_w were obtained from linear interpolation of the relevant 3 dB bandwidth values given by Harris (1978).

3. Results

A total of 18 targets of length 91–477 mm were produced and measured (Table 1). The density of the target material (PVA-C) was 1036 kg m^{-3} and average sound speed in the PVA-C was 1540.3 m s^{-1} (Table 3). The sound speed in water during PVA-C sound speed measurements was 1482.0 m s^{-1}. The average of the daily estimates of seawater sound speed at the target depth was 1494.1 (± 1.5) m s^{-1}.

The ability to detect and identify echoes from the target boundaries varied mostly with pulse bandwidth and power taper setting and was most easily achieved when the target was observed at or close to the broadside aspect (Figs. 4, 5). In general, the 160 – 260 kHz band was better than the 45 – 90 kHz band and the slow power taper performed better than the fast (e.g., Fig. 5). To elaborate, for plain targets, 72 % of length and 94 % of width measurement attempts were successful with the 160 – 260 kHz pulse compared to 28 % and 72 % with the 45 – 90 kHz pulse (Fig. 5). Similarly, for a slow tapered 160 – 260 kHz pulse, 78 % of length and all of the width measurements were successful

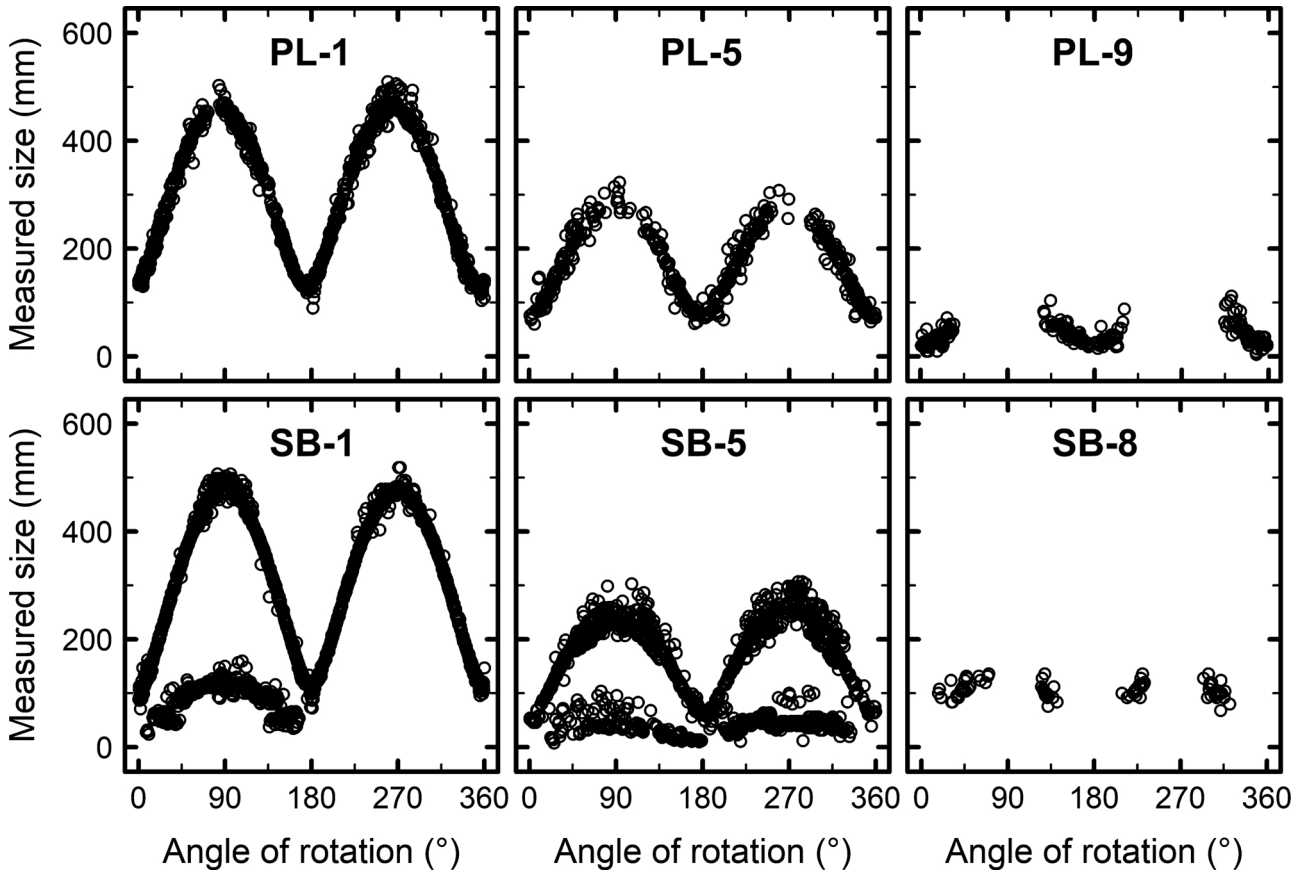

Fig. 4. Estimates of acoustically measured apparent target and cavity size perpendicular to the acoustic beam obtained from three plain targets (upper row) and three targets with cavities (lower row), as a function of rotation angle, using a slow tapered 160-260 kHz pulse. Each plot contains data from three rotations of the respective target.

compared to 67 % and 89 % when using a fast taper (Fig. 5C–D). The lowest success rates occurred when the tips of the target were facing the transducers. There was a slight non-symmetry in the target shape at the tips due to the mould casting procedure and this resulted in a small non-symmetry in the echo data when the target was end-on.

The plain target body widths were measured well by both echo-sounders (Fig. 5). Targets of width greater than about 50 mm could be measured with 45 – 90 kHz pulses (Fig. 5A–B) and those greater than about 20 mm with the 160 – 260 kHz pulses (Fig. 5C–D). Only cavity-bearing targets with widths greater than 40 mm could be measured, and then only at 160 – 260 kHz (Fig. 6A).

The length of targets above about 200 mm could be measured with 160 – 260 kHz pulses (Figs. 5C, 6A). At 45 – 90 kHz, only targets greater than about 320 mm could be measured for length (Fig. 5A–B) due to the weak reflection from the target tips observed for < 320 mm long targets (where the SNR became less than 8 dB). The cavity length measures could only be extracted when the cavity length was greater than 80 mm (Figs. 4, 6B). The success in cavity boundary detection varied with rotation angle (e.g., Figs. 4 and 3). Cavity width could not be extracted, regardless of target size or pulse parameter.

The proportion of pings from which it was possible to obtain a size estimate was highest (0.4 – 0.9) when measuring the width of plain targets. This compares to 0.1 – 0.4 and 0.3 – 0.6 for cavity bearing target width and length measures respectively, and 0.2 – 0.5 for plain target length measures. The 160 – 260 kHz slow tapered pulse was generally most effective at resolving closely-spaced echoes. At

Table 3
PVA-C sound speed and density measurements and selected examples of fish flesh sound speed for comparison, as is the specific acoustic impedance (sound speed multiplied by density). Where a density value was not available, a value of 1036 kg m^{-3} was used for the targets and 1035.5 kg m^{-3} for the fishes. The midpoint of sound speed and density ranges were used when calculating the specific acoustic impedances.

Target ID	Sound speed [m s^{-1}]	Standard deviation of sound speed [m s^{-1}]	Number of sound speed measurements	Density [kg m^{-3}]	Specific acoustic impedance [kg m^{-2} s^{-1}]
PL-1	1534.4	0.9	9	–	1.590×10^6
PL-2	1540.5	1.1	9	1036	1.596×10^6
PL-3	1545.7	1.1	9	1036	1.601×10^6
PL-4	1540.7	2.0	9	1036	1.596×10^6
Mackerel[a]	1528 – 1554			–	$\approx 1.596 \times 10^6$
Lanternfish[b]	1514 – 1522			1027 – 1044	$\approx 1.572 \times 10^6$
Cod[c]	1502 – 1536			–	$\approx 1.573 \times 10^6$

[a] Sound speed in tissue of *Scomber scombrus* at 5–15 °C and ~10 % fat content (Sigfusson et al., 2001).
[b] Sound speed for whole bodies of *Stenobrachius leucopsarus* at 5–15 °C (Yasuma et al., 2006).
[c] Sound speed in filets of *Gadus morhua* at 5–15 °C (Ghaedian et al., 1997).

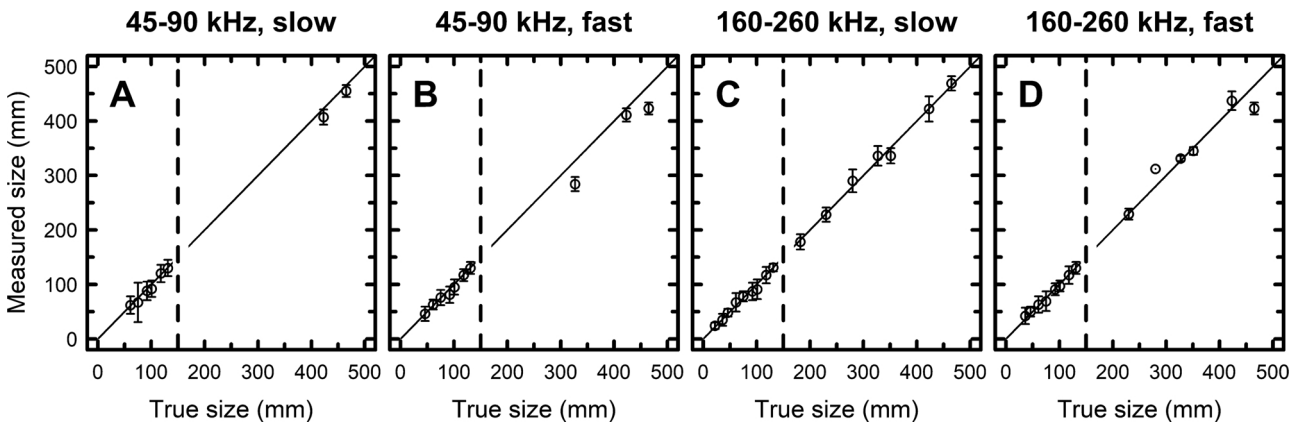

Fig. 5. Acoustically derived estimates of plain target sizes for the four pulse types used, compared to the true size. Width estimates are shown to the left of the vertical dashed line and length estimates to the right. Error bars are ± 1 standard deviation.

160 – 260 kHz, accepted PVA/C-seawater boundary detections at broadside aspect (target width) had a SNR between 15 and 27 dB for 91 – 280 mm long targets and between 28 and 37 dB for targets longer than 280 mm. Similarly, accepted PVA/C-seawater boundary detections at tip-on aspect (target length) had a SNR of 8–15 dB for 182 – 280 mm long targets and 9–23 dB for targets longer than 280 mm. A SNR greater than 20 dB was observed for cavity boundary detections (tip-on aspect only).

The target size estimates were most accurate for width measurements – the root-mean-square (RMS) of the difference between the acoustic and true measurements was 12 mm for plain and 9 mm for cavity-bearing targets. Corresponding values for the length were 17 mm and 16 mm. There were no clear patterns in RMS variability with the target size. For the slow tapered 160-260 kHz pulses the distribution of errors was symmetrical and slightly underestimated the true length (Fig. 7). The range resolution of pulse compressed broadband signals as a function of the pulse bandwidth and taper duration varied from 6.6–24 mm for the pulses and tapers used (Fig. 8).

4. Discussion

The good performance of the slow tapered 160 – 260 kHz pulse (Figs. 4–7), rather than the fast pulse with a higher range resolution, occurred for two reasons; 1) higher bandwidth pulses have a higher range resolution (Fig. 8), and 2) slow tapering gives considerably lower temporal sidelobes which, for closely-spaced echoes, more than compensated for the reduced range resolution of a slow taper.

Sizing accuracy was higher for broadside observations compared to end-on, despite the smaller distance being measured. This occurred because the end-on aspect presented a very small and highly sloped surface towards the acoustic beam – detecting this accurately was difficult at times. In comparison, the broadside aspect produced a strong echo due to the relatively large surface area perpendicular to the beam. However, smaller targets were sized as accurately as the large (Figs. 5–6) provided the target boundaries could be detected and tracked in the first place. The method was not able to estimate size when echoes were too weak compared to the background noise level or were obscured by adjacent scatterers, such as the cavity in some of the targets.

Plain targets were generally easier to measure, and the size could be obtained for smaller targets than with cavity-bearing targets. The presence of a cavity made it more challenging to detect and track echoes from the external boundaries of the targets due to the presence of temporal sidelobes from the cavity echoes.

The method tested did not return satisfactory results in three cases: i) the target boundary signal-to-noise ratio was not high enough for reliable detection and tracking, ii) target boundaries were too close to each other to be separated as distinct signals, and iii) when strong cavity echoes 'masked' the adjacent weaker target echoes. The targets were intentionally made of a material with an acoustic impedance that was similar to fish flesh (e.g., Shibata, 1970; Yasuma et al., 2009; Becker and Warren, 2015) and down to sizes that were unlikely to be resolvable with the range resolution of the 45 – 90 kHz pulse. This is clearly illustrated by the 45 – 90 kHz pulse being unable to detect the smaller targets when viewed end-on, whereas the same target could be detected and accurately sized with the 160 – 260 kHz pulse (Fig. 5). The

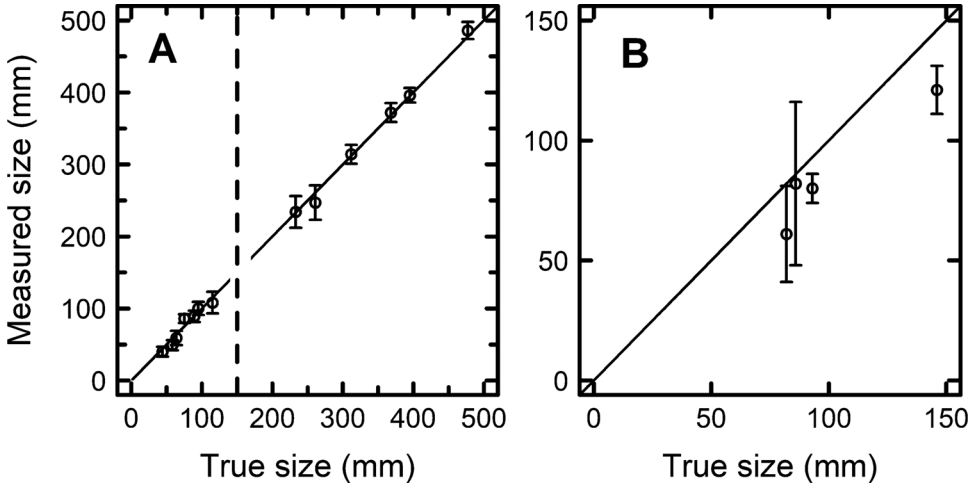

Fig. 6. Acoustically derived size estimates of targets with a cavity compared to the true size for a slow tapered 160-260 kHz pulse. A: target width estimates are shown to the left of the vertical dashed line and target length to the right. B: cavity length measurements (measurement of cavity width was not possible). Error bars are ± 1 standard deviation.

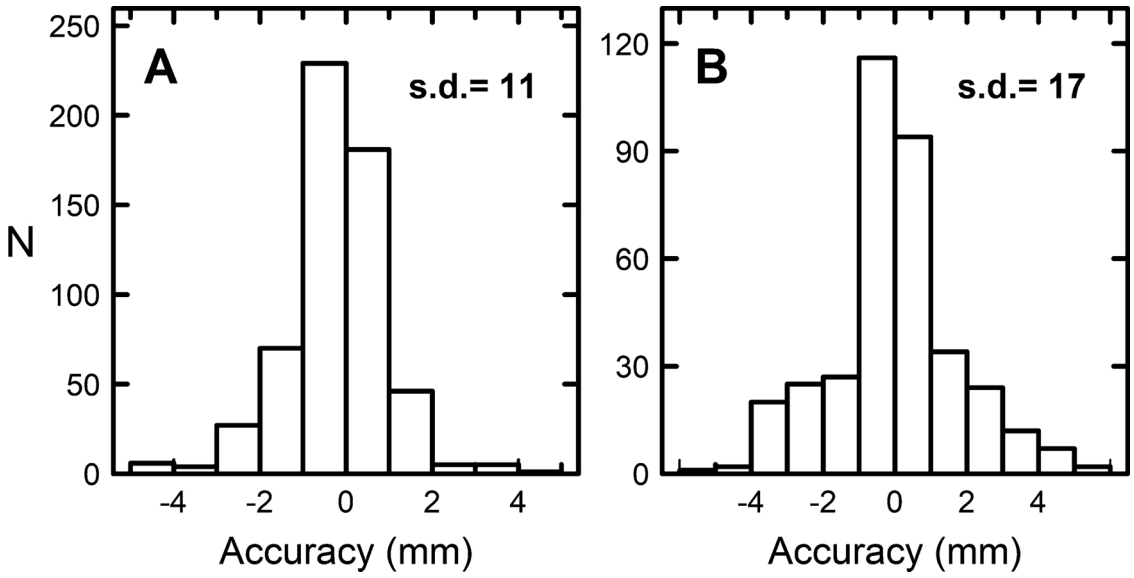

Fig. 7. Distribution of target sizing accuracy defined as the true size subtracted from the measured size for target width (A) and length (B). Data were pooled from all slow taper 160-260 kHz measurements. The standard deviation (s.d.) of each distribution is shown.

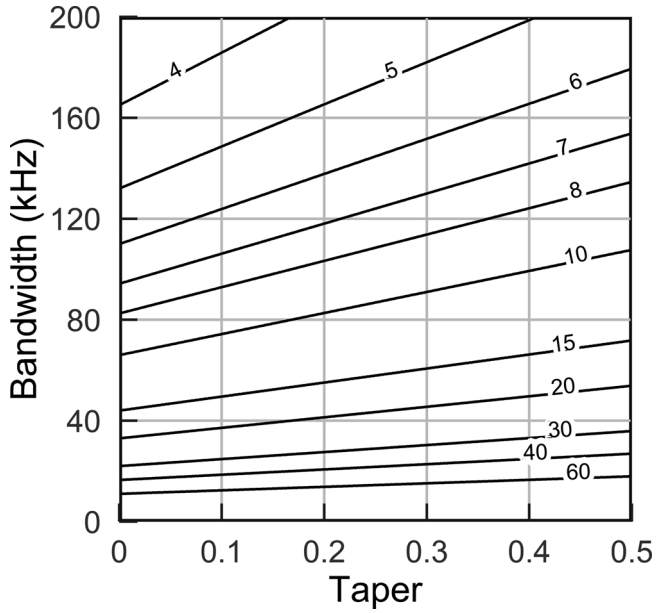

Fig. 8. Range resolution (mm) of linear frequency modulated broadband pulses as a function of taper and pulse bandwidth. Taper of 0.5 means that 50 % of the pulse duration is used to reach maximum transmit amplitude.

width of the smaller targets was less than twice the range resolution of the 45 – 90 kHz pulse (Fig. 5A–B, Fig. 8) and could not be measured. The range resolution of the 160 – 260 kHz pulse, however, was always finer than the width of the smallest target and the width was always able to be estimated (Fig. 5C). The pulse compression temporal sidelobes from the cavity echo were sufficiently strong that the echo from the PVA-C/seawater boundary at broadside was completely (45 – 90 kHz) or almost completely (160 – 260 kHz, Fig. 9) obscured even for the largest cavity-bearing target. In some situations, the cavity echo would shadow the PVA-C/seawater boundary behind the cavity.

The sizing accuracy did not vary between fast and slow pulse tapers when the target boundary echoes were above the background noise, were sufficiently separated (at least twice the estimated range resolution, Fig. 8), and were not close to other strongly reflecting boundaries (such as an air-filled cavity). This was the case for the plain targets at broadside (Fig. 5A vs. B and C vs. D). In contrast, the slow taper is beneficial for targets with an air-filled cavity due to the lower amplitude of the pulse compression sidelobes (Fig. 9).

The nominal range resolution is higher for fast tapering given the same signal bandwidth (Fig. 8). However, the temporal sidelobes in pulse compressed signals are also most prominent for the fast taper and can adversely influence the ability to detect close target echoes (e.g., Fig. 9).

The effective range at sea of the 160 – 260 kHz pulse is about 150 m, which may be too short for the potential application of remotely sizing fish prior to catching with a purse seine. In contrast, the 45 – 90 kHz pulse has an effective range that is more useful for purse seine fishing (some 500 m), but with a significantly lower range resolution (15 and 24 mm for fast and slow tapers). If this trade-off in range resolution for operating range is not suitable, an intermediate frequency range could be chosen, such as the commonly available 90 – 160 kHz. Transducers with narrow beam-widths must also be considered as high range resolution alone may not be adequate for inspection of individual fishes at distance when target densities are high.

Sizing of fish with broadband acoustic pulses has a realistic potential, as demonstrated by the measurements on fish-like targets presented in this paper. The slow pulse taper will likely be most useful when measuring fish with gas-filled swimbladders despite the lower range resolution (Fig. 9). The higher the echosounder frequency the higher the available bandwidth and hence higher range resolutions can be achieved. However, these higher frequencies have a shorter operating range. The further the distance to the fish, the lower the sounder frequency that is needed to achieve an adequate signal-to-noise ratio in the echo and hence only larger fish can be sized. For example, we anticipate that there is potential to size fish such as Atlantic herring (*Clupea harengus*) and mackerel (*Scomber scombrus*) by using a sideways-pointing narrow beam-width transducer operating with a frequency bandwidth that achieves adequate range resolution to the necessary range. Similarly, fish body height measurement should be feasible with downwards oriented transducers. This is perhaps especially so for fishes of comparatively low schooling densities, such as Atlantic cod (*Gadus morhua*) and haddock (*Melanogrammus aeglefinus*). These fishes are frequently resolved as individual targets up to a few hundred meters depth by conventional ship-mounted echosounders operating at frequency bandwidths tested in our study. Lastly, organism size estimates without biological sampling are of special relevance to autonomous platforms such as surface and underwater drones.

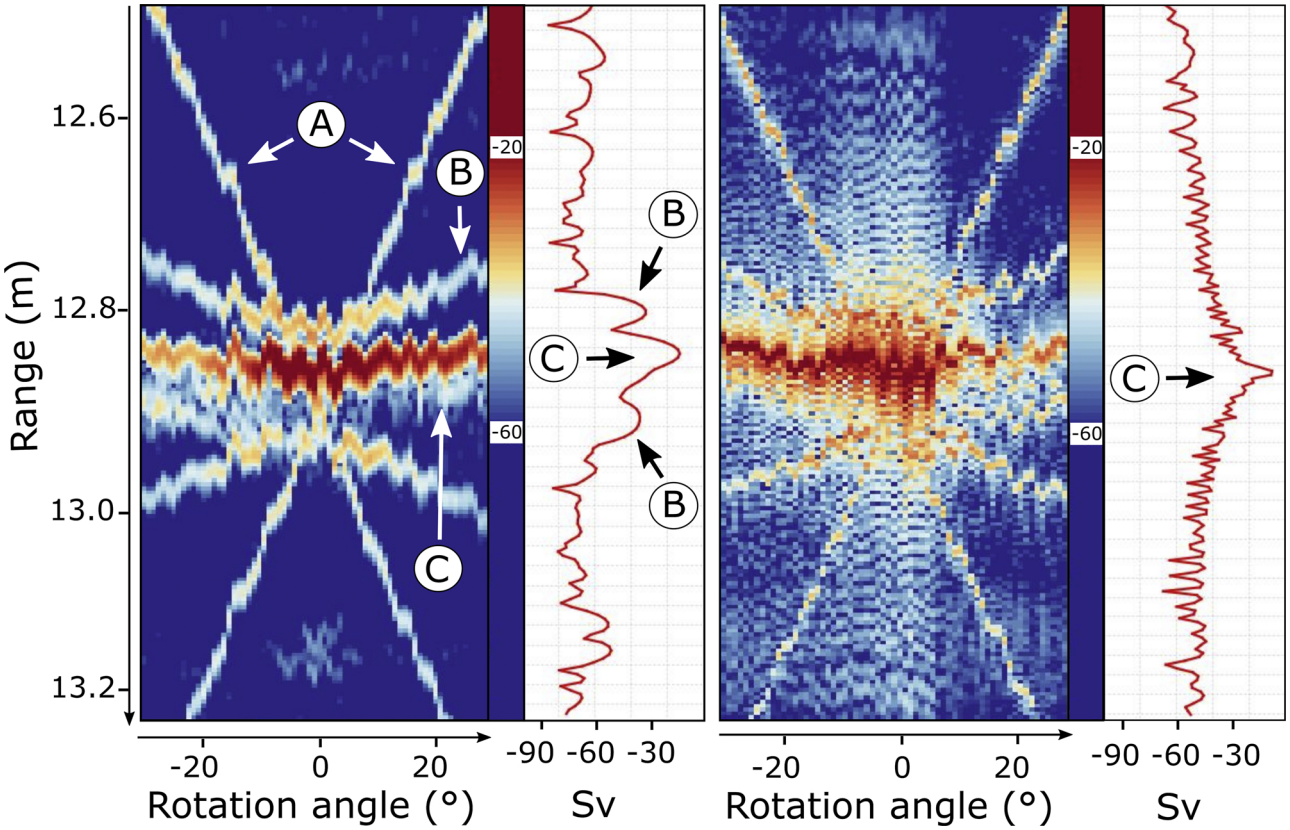

Fig. 9. Illustrative echograms from target SB-1 at broadside aspect (±30°) using a 160-260 kHz slow (left) and fast (right) tapered pulse. The amplitude at rotation angle 0° (broadside) is drawn to the right of each echogram. Vertical suspension lines (A), PVA-C to seawater boundaries (B) and cavity (C) are labelled. Echogram colour scale and line plot show volume backscatter strength (S_v, dB re 1 m^{-1}).

The method used worked well with the clearly defined PVA-C/seawater boundaries. Fish flesh-to-seawater boundary echoes may, however, not be as clear due to the abundance of confounding sound scattering structures inside the fish (e.g., bones). In this case, we anticipate that where clear and isolated echo peaks from the outer boundaries of the fish are not present the overall length of the echo could be used to estimate the fish size.

Aspects not considered in this work, but which would be necessary to address for operational sizing include the determination of fish species and fish orientation to the acoustic beam. We envision that species identification would be provided via other means, such as acoustic frequency response (e.g., Korneliussen, 2018) and non-acoustic means such as location, time of year, and depth of fish. Tracking of fish over several pings can be used to estimate fish orientation (see e.g., Furusawa and Miyanohana, 1990; Chu et al., 2003; Handegard, 2007; Jaffe and Roberts, 2011). A simpler method, however, could be applied to purse seine fishing. Here, pre-catch inspection of schools with omni-directional fisheries sonars is routine; the vessel circles the school a few times at some distance in order to determine the size, depth and shape of the school (e.g., Vatnehol et al., 2016). A laterally observing, narrow acoustic beam could be aimed at the school at the same time and resolve single fish echoes in the outskirts of the school. A variety of fish orientations would be observed, and a distribution of apparent fish sizes obtained. The extremities of this distribution are anticipated to correspond to the fish body width and length. If the acoustic beam is instead vertical, the challenge becomes to measure the height of fish with only the fish tilt angle affecting the apparent height. This approach may be practicable for vertically-oriented echosounders such as on the hull of fishing vessels, on a trawl headline, or on probes deployed from research vessels. We also note that the smallest object that we could detect was generally limited by the range resolution. Smaller objects could be measured by using a higher bandwidth pulse, but this would reduce the working range of the system. In some situations, such as from trawls and probes, this reduced working range would not be problematic.

In this study, it was demonstrated that pulse compressed broadband signals can be used to directly and remotely size fish-flesh like targets that have dimensions similar to typical medium-sized fishes (15 – 75 cm). The target boundaries could be resolved, tracked, and converted into estimates of target size. Air-filled cavities had a detrimental effect on sizing success. The results provide promise that the method will also be effective on real fish.

CRediT authorship contribution statement

Rokas Kubilius: Conceptualization, Methodology, Investigation, Formal analysis, Writing - original draft, Visualization. **Gavin J. Macaulay:** Conceptualization, Methodology, Investigation, Writing - review & editing, Visualization. **Egil Ona:** Conceptualization, Methodology, Investigation, Writing - review & editing.

Declaration of Competing Interest

None.

Acknowledgements

The experimental work was funded by the Research Council of Norway under the AcoSize project (no. 255589/E40). We are grateful to Austevoll Research Station (Norway) personnel for their assistance during the work. Rune Øyerhamn (NORCE, Norway) is thanked for his contribution to the target material sound speed measurements. Atle Totland (IMR, Norway) is thanked for his skilful design, construction and operation of the target rotation apparatus.

References

Au, W.W.L., Benoit-Bird, K.J., 2003. Acoustic backscattering by Hawaiian lutjanid snappers. II. Broadband temporal and spectral structure. J. Acoust. Soc. Am. 114, 2767–2774. https://doi.org/10.1121/1.1614257.

Becker, K.N., Warren, J.D., 2015. Material properties of Pacific hake, Humboldt squid, and two species of myctophids in the California current. J. Acoust. Soc. Am. 137, 2522–2532. https://doi.org/10.1121/1.4919308.

Belcher, E., Matsuyama, B., Trimble, G., 2001. Object identification with acoustic lenses. MTS/IEEE Oceans 2001. An Ocean Odyssey. Conference Proceedings (IEEE Cat. No.01CH37295) 6–11. https://doi.org/10.1109/OCEANS.2001.968656.

Briseño-Avena, C., Roberts, P.L.D., Franks, P.J.S., Jaffe, J.S., 2015. ZOOPS- O2: a broadband echosounder with coordinated stereo optical imaging for observing plankton in situ. Methods Oceanogr. 12, 36–54. https://doi.org/10.1016/j.mio.2015.07.001.

Chan, V., Perlas, A., 2011. Basics of ultrasound imaging. In: Narouze, S.N. (Ed.), Atlas of Ultrasound-Guided Procedures in Interventional Pain Management. Springer, New York, pp. 13–19. https://doi.org/10.1007/978-1-4419-1681-5_2.

Chu, D., Wiebe, P., Copley, N., 2000. Inference of material properties of zooplankton from acoustic and resistivity measurements. ICES J. Mar. Sci. 57, 1128–1142. https://doi.org/10.1006/jmsc.2000.0800.

Chu, D., Jech, J.M., Lavery, A., 2003. Inference of geometrical and behavioural parameters of individual fish from echo-trace-analysis. Deep. Sea Res. Part I Oceanogr. Res. Pap. 50, 515–527. https://doi.org/10.1016/S0967-0637(03)00035-9.

Chu, D., Jech, J.M., Tomich, S.D., Hufnagle, L.C., 2015. A high-resolution acoustic imaging system to map interior fish morphology. Mar. Technol. Soc. J. 49, 59–69. https://doi.org/10.4031/MTSJ.49.2.8.

Cook, C.E., Bernfeld, M., 1967. Radar Signals: An Introduction to Theory and Application. Academic Press. 550 pp. https://doi.org/10.1016/B978-0-12-186750-8.X5001-7.

Demer, D.A., Berger, L., Bernasconi, M., Bethke, E., Boswell, K., Chu, D., Domokos, R., et al., 2015. Calibration of Acoustic Instruments. ICES Cooperative Research Report No. 326. 133 pp. https://doi.org/10.25607/OBP-185.

Ehrenberg, J.E., Torkelson, T.C., 2000. FM slide (chirp) signals: a technique for significantly improving the signal-to-noise performance in hydroacoustic assessment systems. Fish. Res. 47, 193–199. https://doi.org/10.1016/S0165-7836(00)00169-7.

Fofonoff, N.P., Millard Jr., R.C., 1983. Algorithms for the computation of fundamental properties of seawater. UNESCO Tech. Pap. Mar. Sci. 44, 53 pp. http://hdl.handle.net/11329/109.

Forland, T.N., Hobæk, H., Korneliussen, R.J., 2014. Scattering properties of Atlantic mackerel over a wide frequency range. ICES J. Mar. Sci. 71, 1904–1912. https://doi.org/10.1093/icesjms/fsu045.

Francois, R.E., Garrison, G.R., 1982. Sound absorption based on ocean measurements. Part II: Boric acid contribution and equation for total absorption. J. Acoust. Soc. Am. 72 (6), 1879–1890. https://doi.org/10.1121/1.388673.

Furusawa, M., Miyanohana, Y., 1990. Behaviour and target-strength observation through echo traces of individual fish. Rapp. P.-v. Réun. Cons. Int. Explor. Mer 189, 283–294.

Ghaedian, R., Decker, E.A., McClements, D.J., 1997. Use of ultrasound to determine cod fillet composition. J. Food Sci. 62, 500–504. https://doi.org/10.1111/j.1365-2621.1997.tb04415.x.

Handegard, N.O., 2007. Observing individual fish behavior in fish aggregations: tracking in dense fish aggregations using a split-beam echosounder. J. Acoust. Soc. Am. 122, 177–187. https://doi.org/10.1121/1.2739421.

Handegard, N.O., Patel, R., Hjellvik, V., 2005. Tracking individual fish from a moving platform using a split-beam transducer. J. Acoust. Soc. Am. 118, 2210–2223. https://doi.org/10.1121/1.2011410.

Harris, F.J., 1978. On the use of windows for harmonic analysis with the discrete Fourier transform. Proc. IEEE 66, 51–83. https://doi.org/10.1109/PROC.1978.10837.

Hawkins, D.W., 1996. Synthetic Aperture Imaging Algorithms: With Application to Wide Bandwidth Sonar. Ph.D. thesis. University of Canterbury. http://hdl.handle.net/10092/1082.

Huse, I., Vold, A., 2010. Mortality of mackerel (Scomber scombrus L.) after pursing and slipping from a purse seine. Fish. Res. 106, 54–59. https://doi.org/10.1016/j.fishres.2010.07.001.

Imaizumi, T., Furusawa, M., Akamatsu, T., Nishimori, Y., 2008. Measuring the target strength spectra of fish using dolphin-like short broadband sonar signals. J. Acoust. Soc. Am. 124, 3440–3449. https://doi.org/10.1121/1.2990703.

Jaffe, J.S., 2006. Using multi-angle scattered sound to size fish swimbladders. ICES J. Mar. Sci. 63, 1397–1404. https://doi.org/10.1016/j.icesjms.2006.04.024.

Jaffe, J.S., Roberts, P.L.D., 2011. Estimating fish orientation from broadband, limited-angle, multiview, acoustic reflections. J. Acoust. Soc. Am. 129, 670–680. https://doi.org/10.1121/1.3523430.

Korneliussen, R.J. (Ed.), 2018. Acoustic Target Classification. ICES Cooperative Research. Report No. 344. 104 pp. http://doi.org/10.17895/ices.pub.4567.

Korneliussen, R.J., Heggelund, Y., Macaulay, G.J., Patel, D., Johnsen, E., Eliassen, I.K., 2016. Acoustic identification of marine species using a feature library. Methods Oceanogr. 17, 187–205. https://doi.org/10.1016/j.mio.2016.09.002.

Macaulay, G.J., 2002. Anatomically detailed acoustic scattering models of fish. Bioacoustics 12, 275–277. https://doi.org/10.1080/09524622.2002.9753720.

Shibata, K., 1970. Study on details of ultrasonic reflection from individual fish. Bull. Faculty Fish. Nagasaki Univ. 29, 1–82.

Sigfusson, H., Decker, E.A., McClements, D.J., 2001. Ultrasonic characterization of Atlantic mackerel (Scomber scombrus). Food Res. Int. 34, 15–23. https://doi.org/10.1016/S0963-9969(00)00123-X.

Simmonds, E.J., MacLennan, D.N., 2005. Fisheries Acoustics: Theory and Practice. Blackwell Science, Oxford. 437 pp. https://doi.org/10.1002/9780470995303.

Söhnlein, G., Rush, S., Thompson, L., 2011. Using Manned Submersibles to Create 3D Sonar Scans of Shipwrecks. OCEANS'11 MTS/IEEE KONA, pp. 1–10. https://doi.org/10.23919/OCEANS.2011.6107130.

Stanton, T.K., Reeder, D.B., Jech, J.M., 2003. Inferring fish orientation from broadband-acoustic echoes. ICES J. Mar. Sci. 60, 524–531. https://doi.org/10.1016/S1054-3139(03)00032-8.

Stanton, T.K., Lee, W.-J., Baik, K., 2018. Echo statistics associated with discrete scatterers: a tutorial on physics-based methods. J. Acoust. Soc. Am. 144, 3124–3171. https://doi.org/10.1121/1.5052255.

Surry, K.J., Austin, H.J.B., Fenster, A., Peters, T.M., 2004. Poly(vinyl alcohol) cryogel phantoms for use in ultrasound and MR imaging. Phys. Med. Biol. 49, 5529–5546. https://doi.org/10.1088/0031-9155/49/24/009.

Tenningen, M., Vold, A., Olsen, R.E., 2012. The response of herring to high crowding densities in purse-seines: survival and stress reaction. ICES J. Mar. Sci. 69, 1523–1531. https://doi.org/10.1093/icesjms/fss114.

Vatnehol, S., Peña, H., Ona, E., 2016. Estimating the volumes of fish schools from observations with multi-beam sonars. ICES J. Mar. Sci. 74, 813–821. https://doi.org/10.1093/icesjms/fsw186.

Watson, R., Revenga, C., Kura, Y., 2006. Fishing gear associated with global marine catches: I. Database development. Fish. Res. 79, 97–102. https://doi.org/10.1016/j.fishres.2006.01.010.

Yasuma, H., Takao, Y., Sawada, K., Miyashita, K., Aoki, I., 2006. Target strength of the lanternfish, Stenobrachius leucopsarus (family Myctophidae), a fish without an air-bladder, measured in the Bering Sea. ICES J. Mar. Sci. 63, 683–692. https://doi.org/10.1016/j.icesjms.2005.02.016.

Yasuma, H., Nakagawa, R., Yamakawa, T., Miyashita, K., Aoki, I., 2009. Density and sound-speed contrasts, and target strength of Japanese sandeel Ammodytes personatus. Fish. Sci. 75, 545–552. https://doi.org/10.1007/s12562-009-0091-3.